Biomimetic functionalization with leukocyte membranes imparts cell like functions to synthetic particles

Alessandro Parodi, Nicoletta Quattrocchi, Anne L. van de Ven, Ciro Chiappini, Michael Evangelopoulos, Jonathan O. Martinez, Brandon S. Brown , Sm Z. Khaled, Iman K. Yazdi, Maria Vittoria Enzo, Lucas Isenhart, Mauro Ferrari, Ennio Tasciotti

1. The Leukolike Vector (LLV)

The LLV were engineered using a nanoporous silicon core (**Supplementary figure 1A**) and coated with purified cellular membranes derived from leukocyte cells (**Supplementary figure 1B**). The assembly relied on NPS surface chemical functionalization to produce a uniform leukocyte coating (**Supplementary figure 1C, Supplementary figure S6**). Membrane coated NPS enabled avoidance of opsonization (**Supplementary figure 1D**), avoidance of internalization by mononuclear phagocytic cells (**Supplementary figure 1E**), and increased endothelial permeability (**Supplementary figure 1F**). The addition of a leukocyte-derived coating to the NPS allowed for the negotiation of the vasculature related barrier.

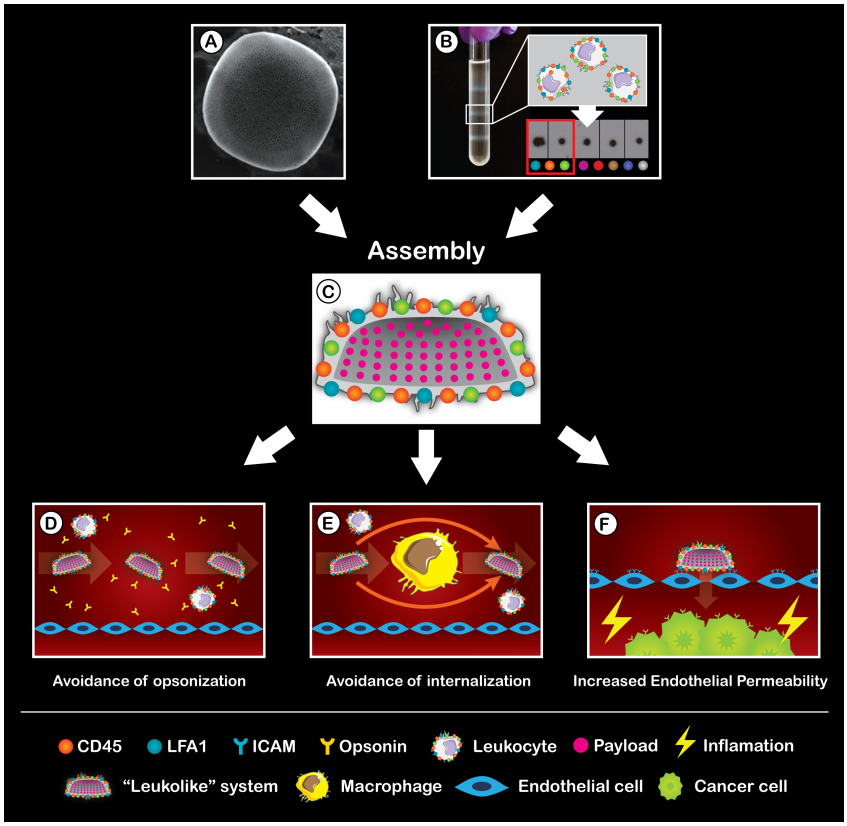

Supplementary figure S1. Luekolike Vector assembly to overcome vasculature related barrier. A. SEM image of nanoporous silicon core **B.** Ultracentrifugation picture depicting fraction of interest with dot blot comparison **C.** LLV image with NPS core and leukocyte coating **D-F.** LLV ability to avoid opsonization

2. Isolation of the leukocyte membrane

The isolation of the cellular membrane was performed through a discontinuous sucrose gradient. The gradient was divided in ten different fractions (**Supplementary figure S2A**) and analyzed for extracellular membrane biomarkers (CD45, LcK, LFA-1 and CD3z) and cytoplasmic biomarker (Np 62 and COX IV) through dot blot (**Supplementary figure S2B**). Fractions 5 and 6 were identified and chosen as enriched in extracellular membrane.

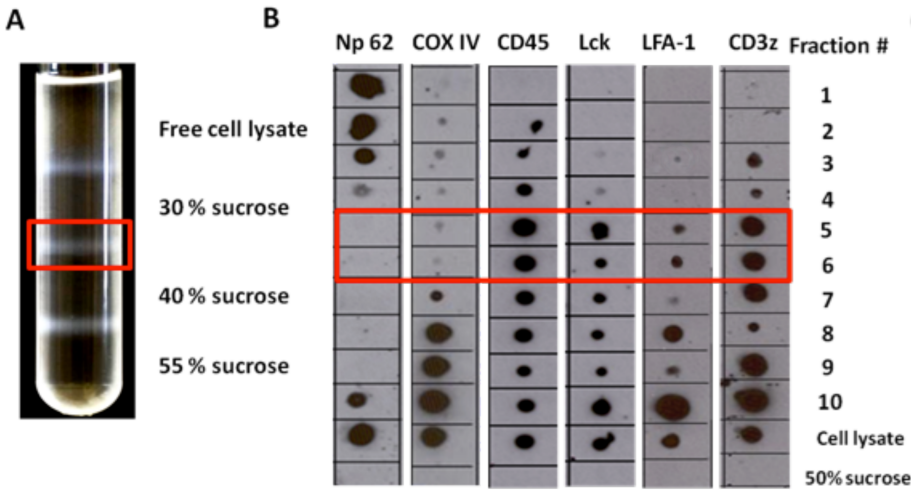

Supplementary figure S2. Purification of leukocyte membranes through discontinuous density sucrose gradient. A. A discontinuous sucrose gradient (55-40-30 % sucrose (w/v)) with free-cell lysate layered on top of the 30 % sucrose solution as it appeared after ultracentrifugation. Three lipid rings localized at the interfaces of the different sucrose solution were clearly detectable. **B**. Immunoblotting for leukocyte cellular membrane marker-proteins relative to different cellular compartments to select the fractions enriched only with plasmacellular membranes: Nucleoporin 62 (Np62, nucleus[51]); cytochrome c-oxidase (COX IV , mitochondria[52]); CD45[53,54], lymphocyte-specific protein tyrosine kinase (Lck)[55], LFA-1 and CD3z[56], (plasmacellular membrane). The assembly of the LLV was performed selecting fractions 5 and 6 (both enriched in plasmacellular membranes) corresponding to the lipid ring localized at the 40-30 % sucrose interface (red box) of the sucrose gradient.

3. Characterization of adsorption and molecular interaction between NPS surface and leukocyte membrane

The immobilization of leukocyte membrane on the APTES modified NPS surface and their molecular interactions were characterized by FTIR. As shown in the FTIR spectra in **Supplementary figure S3**, the APTES-NPS displayed peaks at 1059.29 cm^{-1} and 1125 cm^{-1} which originated from the Si-O bond of the silicon surface and Si-O moieties of the APTES molecule respectively[57]. The strong peak at 1617 cm^{-1} represented the bending vibration of APTES aliphatic amine groups (N-H) while the weak spectra in between 2800 and 3000 cm^{-1} corresponded to aliphatic C-H stretching of the APTES backbone conjugated with silicon particles[58]. The symmetric N-H stretching from aliphatic amine of APTES at around 3250 cm^{-1} was vaguely observable because of the existence of a broad peak centered around 3300 cm^{-1}, which derived from the adsorbed water molecules on the silicon. In contrast, the spectra for LLV exhibited a weaker peak for the Si-O moieties and a stronger peak for the C-H stretching compared to that of the APTES-NPS. These bands were due to the immobilization of the

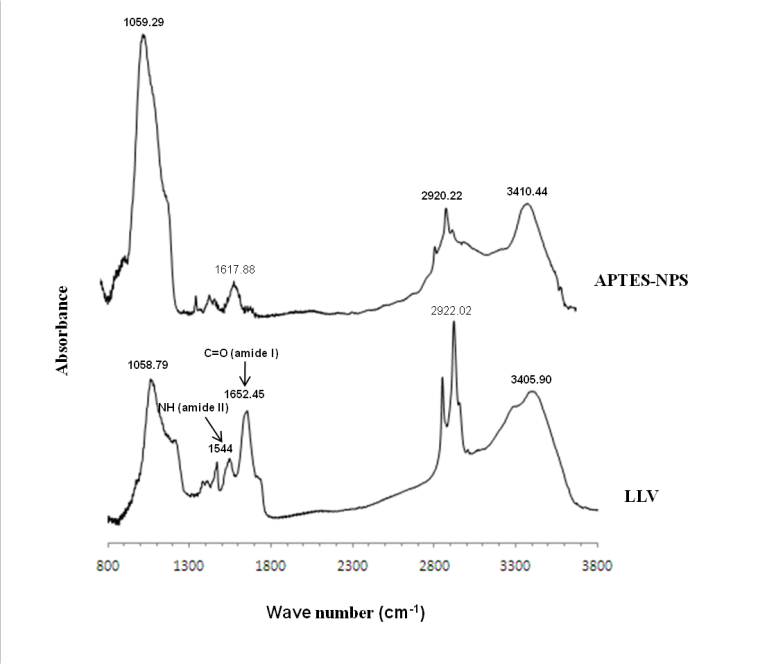

Supplementary figure S3. FTIR spectra of APTES-NPS and LLV. Samples were pressed with KBr to form a pellet before analysis and the spectra were collected by transmitting infrared (IR) light through the pellet. The new peaks at 1544 cm^{-1} and 1652 cm^{-1} on the IR spectra of LLV were the evidence of the immobilization through amide linkage of the membrane proteins onto the APTES modified NPS surface.

membranes on the particle's surface which shielded the silicon surface while exposing the long C-H and C-C chains of phospholipids and proteins. The two strong peaks at 1652 and 1544 cm^{-1} on the LLV spectra corresponded to the amide I and II modes of the proteins of the leukocyte membrane. The amide I band primarily represents the C=O stretching vibrations of the peptide bonds while the amide II band is caused by the C-N stretch coupled with N-H bending mode. This amide linkage arose from the peptide bonds between protein residues and also may result from the covalent bond between the carboxylic moieties of protein and the primary amines of the APTES molecule [59-60]. These bonds may improve the stability of the coating which is principally established by electrostatic forces between lipid bilayer and APTES-NPS surface.

4. Protein Characterization of the LLV and membrane orientation assessment

To characterize LLV's protein content, we investigated the presence of LFA-1 and CD3z, using flow cytometry (**Supplementary figure S4**). The analysis of these two proteins, a transmembrane[61] and an internal membrane protein[62] respectively, provided information on the composition and orientation of the protein pool in the leukocyte membrane and after NPS coating. As a control, the different localization of LFA-1 and CD3z on the extra- and intra-cellular side of the cell membrane was also tested on Jurkat cells, where CD3z was detectable only after membrane permeabilization (**Supplementary figure S4A**). **Supplementary figure S4B** shows the fluorescence intensity of CD3z and LFA-1 associated to LLV obtained with Jurkat membranes (LLV). In this case we compared the coated particles with NPS. The results showed that CD3z level was similar for NPS and LLV, while the signal coming from LFA-1 was three times higher for LLV. Additionally, we tested the presence of CD3z and LFA-1 on the NPS and LLV through dot-blot analysis (**Supplementary figure S4C**). CD3z and LFA-1 were detected on LLV and on the leukocyte membranes (positive control), while no staining was observed for NPS. The results obtained on CD3z through flow cytometry and the immunoblotting confirm not only the presence but also correct protein orientation on the LLV.

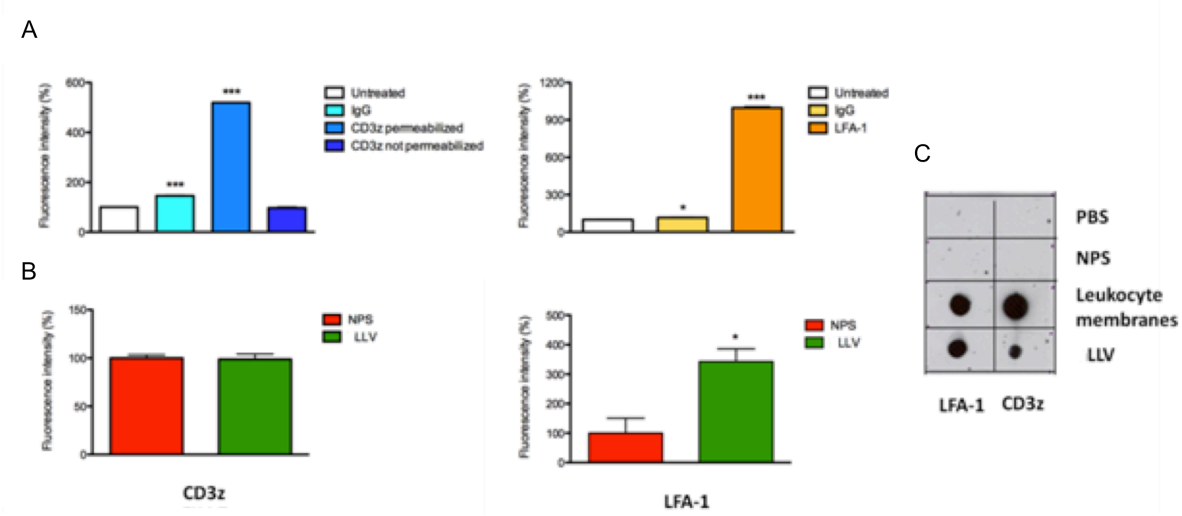

Supplementary figure S4. Protein characterization of the LLV. **A-B**. CD3z and LFA-1expression on Jurkat cells (A) as evaluated through flow cytometry on NPS and LLV (B). Untreated Jurkat cells and IgG were used as negative controls. The standard deviations were obtained from three separate experiments. **C**. Immunoblotting of LFA-1 and CD3z on NPS, leukocyte membranes (positive control) and LLV. PBS was used as a negative control.

5. Stability of the Membrane Coating

The stability of the system was assessed through Thermogravimetric analysis (TGA) after incubation of the LLV in PBS for 1 and 24 hours at 37 °C. As shown in the **Supplementary figure S5**, after heating to nearly and over 100 ºC, LLV lost 70 % of its weight while NPS lost 55 % before reaching the plateau. All weight losses were associated with either the water filling the porous matrix of the NPS or the organic molecules present in the LLV coating. Hence, the 15 % difference between these weight percentages (70-55=15 %) is roughly represented by the amount (in weight) of membrane adsorbed on LLV. Similarly after 24 hours, TGA analysis showed LLV contained 8 wt % membrane. Therefore, 7 % of the membrane was assumed to be lost during storage, corresponding to roughly 40 % of the initial coating. Different degradation rates and patterns were also observed between NPS and LLV through SEM analysis. As shown in the **Supplementary figure S6**, after 1 hour of incubation, there were no changes in the size and overall aspect of both NPS and LLV. At 4 hours NPS were partially degraded but the global

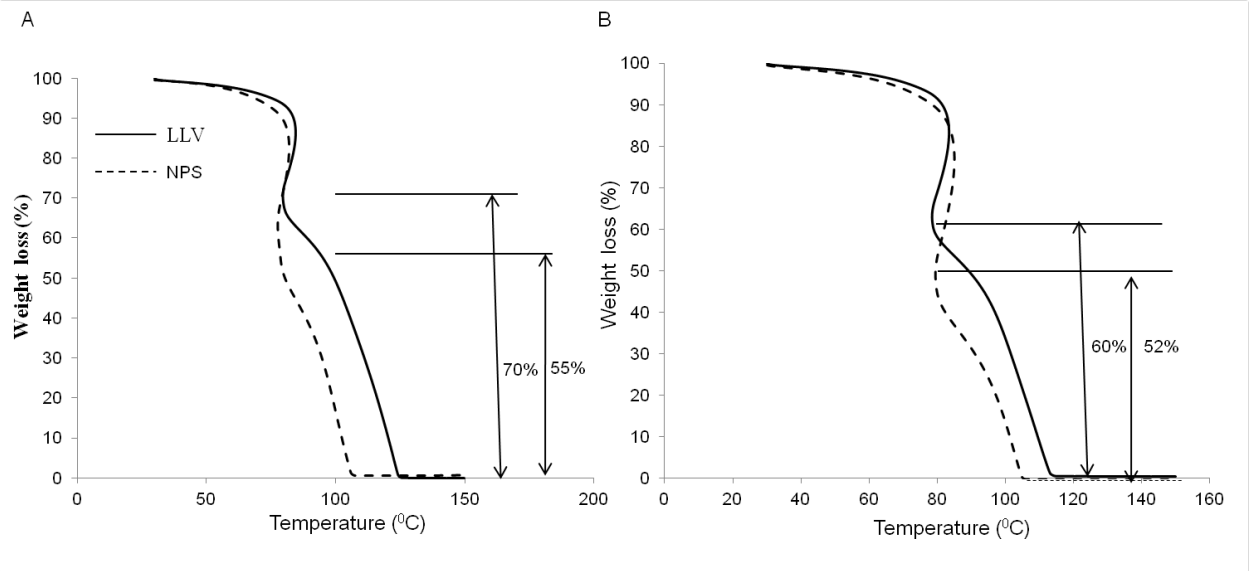

Supplementary figure S5. Thermogravimetric analysis of NPS and LLV. A. 1 hour submersion in PBS and **B.** 24 hour submersion in PBS. TGA was done by heating the particles suspended in water from 30 to 150 ºC at a heating rate of 10 ºC/min. The difference in weight loss between NPS and LLV is roughly representing the wt % of membrane associated with LLV samples. After 1 hour in PBS, the LLV sample contained about 15 wt% membrane while after 24 hour submersion they contained about 8 wt % membrane.

shape was still preserved, while LLV lost a small portion of its coating but there was no evidence of degradation of the underlying porous silicon structure. After 24 hours of treatment, a drastic change in the NPS structure was observed; the external ring degraded completely leaving the inner core collapsed and with the pores practically undistinguishable. The membrane coated LLV fared better. Although most of the coating membranes were lost at the latest time point (showing the pores beneath), the structure of the silicon was preserved. The membrane coating thus increased NPS stability in a physiologic solution and delayed its degradation at early time points.

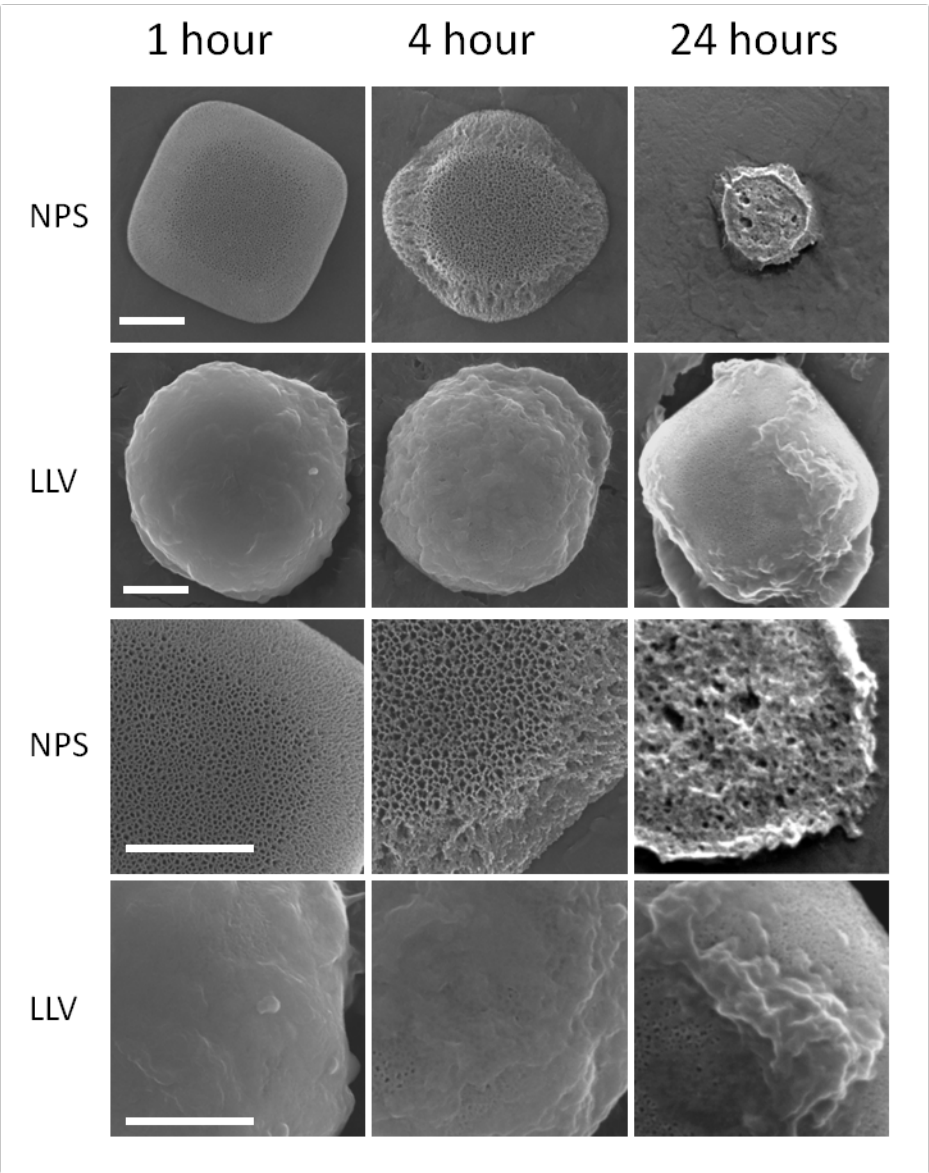

Supplementary figure S6. Degradation Study of NPS and LLV. SEM micrographs showing the degradation process of the NPS in contrast to the stability of the LLV coating over 24 hours, at 37°C in PBS (pH 7.2). Representative close ups of each micrograph are shown in the last two rows. Scale bar = 1 μm

6. LLV loading and release kinetics

NPS were designed to deliver and concentrate, at a given target site, therapeutic cargos such as drug-loaded nanovectors or macromolecules (e.g. siRNA)[63] upon systemic administration as well as exploiting enhanced permeation and retention (EPR) phenomena[64,65]. Surface modifications have been proven to affect the pharmacokinetic profile of different delivery systems and we confirmed those observations by coating silicon with poly-lactic-co-glycolic acid (PLGA) or agarose[66,67]. To verify the modulating action of the membrane coating on the dynamics of drug loading and release, we compared the release profiles of NPS and LLV loaded with comparable amounts of Doxorubicin (DOX) (data not shown). After 3 hours in a cell free environment (particles in PBS at 37 °C), the NPS lost the 50 % of the chemotherapeutic agent against the 20 % lost by the LLV. These results show drug retention by the membrane coating (**Supplementary figure S7A**). After 24 hours (data not shown) both delivery systems completely released their payload, likely as a consequence of membrane coating loss (**Supplementary figure S5**) and the degradation of the porous silicon ultrastructure (**Supplementary figure S6**). The retention of the membrane coating also effectively delayed the release of a biological cargo. FITC-BSA-loaded NPS and LLV showed a similar release trend to the one observed with DOX. In the same conditions, after 3 hours, NPS particles released the 25 % of the loaded cargo, against the 15 % of LLV (**Supplementary figure S7B** left panel).

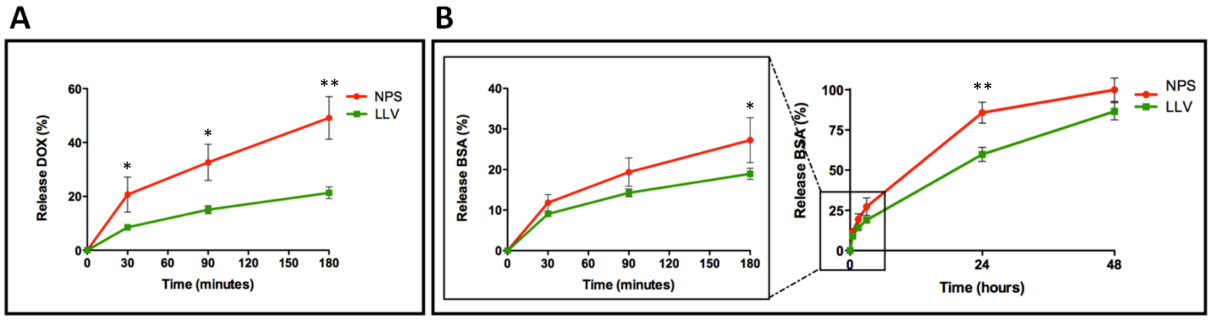

Supplementary figure S7. In vitro DOX and FITC-BSA release profile from NPS and LLV. **A.** Release profile of DOX from NPS and LLV after 30, 90 and 180 minutes in PBS under continuous rotation at 37 °C. At each time point, the amount of released DOX was estimated detecting the absorbance at 480 nm by spectrofluorimetry. **B.** Release profile of FITC-BSA from NPS and LLV in PBS, under continuous rotation at 37 °C. After 180 minutes less than 30 % of the payload was released from both NPS and LLV (left panel). FITC-BSA release was assessed until 48 hours when both the delivery systems released their cargo (right panel). All the data shown are the means ± Standard deviation from three independent experiments. An independent student's t-test was used to compare the groups (* = $p < 0.05$; ** = $p < 0.01$).

Conversely to DOX, FITC-BSA was released slowly from both the systems, reaching a plateau after 48 hours (**Supplementary figure S7B** right panel). The different release profiles of DOX and FITC-BSA could be explained by the formation of covalent bonds between the protein and the surface of the particles, as assessed through FTIR analysis (**Supplementary figure S3**). Moreover, considering the amphipatic nature of BSA, it could hydrophobically interact with the coating on one side[68] and bind the particle surface on the other side, acting as a link between these two components.

7. Observation of Phagocytic-LLV Interactions through Time Lapse Microscopy (TLM)

TLM was performed by treating both human (THP-1) and mouse (J774) phagocytic cells with NPS, J774 LLV and THP-1 LLV. Several random fields of view were observed and macrophage-particle internalization was recorded for more than 4 hours. Exposure of particles to THP-1, a human monocytic cell line, exhibited three distinct responses or interactions (**Supplementary Figure 8A**). As expected, NPS were readily internalized and cells appeared to exhibit ameboid movements actively searching for particles to internalize (**Supplementary movie S1**). On the other hand, cellular coated particles demonstrated significantly different responses where cells exposed to particles coated with mouse macrophage membranes (J774 LLV) displayed a delayed response but eventually resulted in particle internalization **(Supplementary movie S2).** A minor response and lack of pronounced ameboid movements was observed after exposure to particles coated with THP-1 cellular membranes

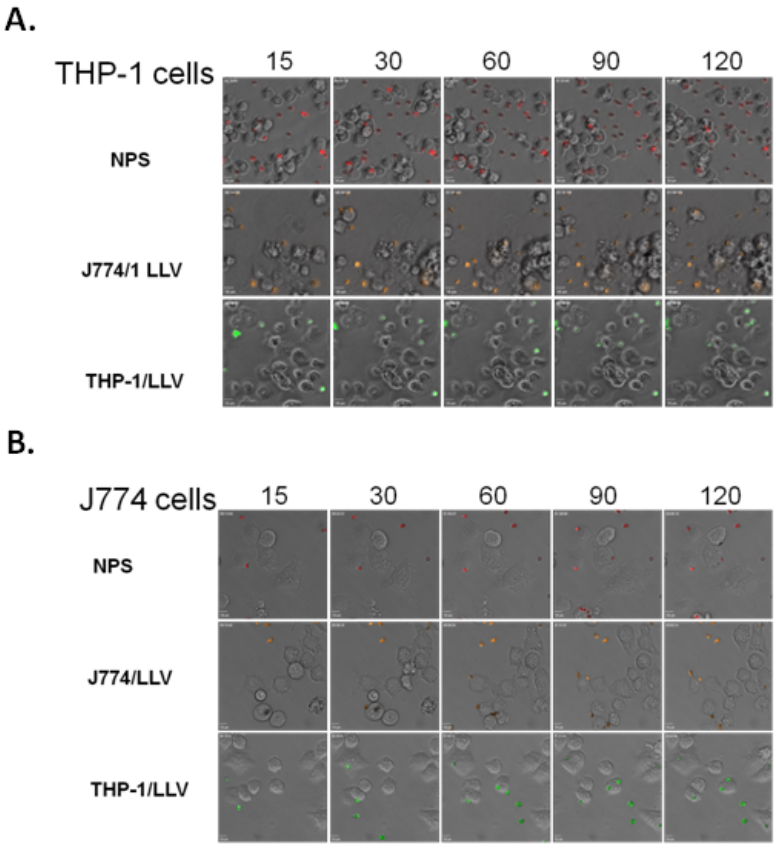

Supplementary figure 8. Human THP-1 phagocytic cells/particles interaction and murine J774 macrophage/particles interaction. A. Representative images of NPS (red), J774 LLV (orange) and THP-1 LLV (green) cultured with THP-1 human monocytic cell line (after incubation with PMA 100 ng/mL; 48h) at various time points taken from time-lapse microscopy of more than 240 minutes of imaging. Selected images were chosen at 15, 30, 60, 90, and 120 minutes. **B.** Representative images of NPS (red), J774 LLV (orange) and THP-1 LLV (green) cultured with murine J774 macrophage cell line (after incubation with PMA 100 ng/mL; 48h) at various time points taken from time-lapse microscopy of more than 240 minutes of imaging. Selected images were chosen at 15, 30, 60, 90, and 120 minutes. Scale bar = 10 µm.

(**Supplementary movie S3**). This result suggested that cellular membranes derived from the same source could impart the ability to avoid internalization from phagocytic cells. A similar setup was used to investigate the interactions with mouse macrophage (J774) cells (**Supplementary Figure 8B**). NPS, as expected, were rapidly internalized and cells displayed pronounced activation and ameboid movements (**Supplementary movie S4**). In this case however, J774 LLV exhibited very minor internalization of particles even after prolonged contact with cell surface (**Supplementary movie S5**). THP-1 LLV showed that a cellular membrane coating could delay but not avoid particle internalization after repetitive interactions with the cells (**Supplementary movie S6**).

8. Cytotoxicity of LLV

In order to study the potential impact of the particles on the cell viability, human THP-1 and murine J774 phagocytic cells were treated for 24 hours with NPS and LLV coated with the membrane of both these cell lines (J774 LLV and THP-1 LLV). The particles did not have any evident impact on the cell viability of both the cell phenotypes (**Supplementary Figure S9**).

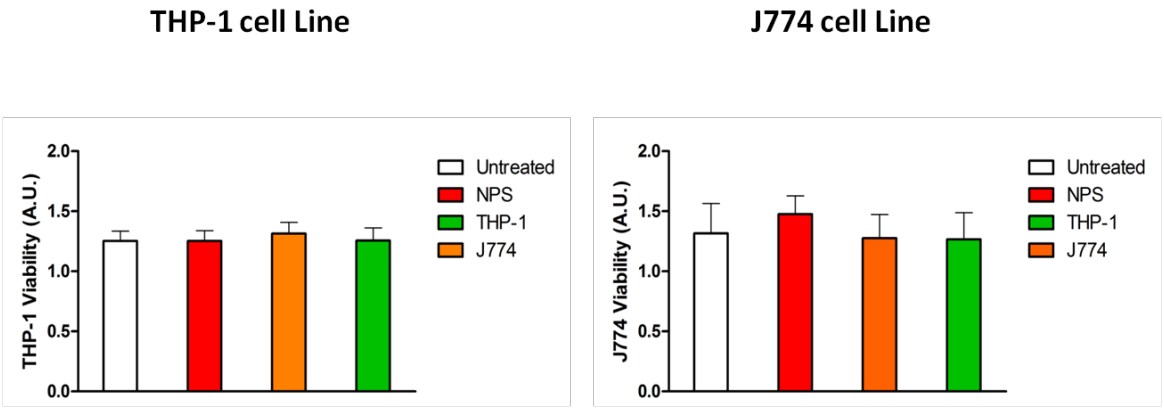

Supplementary figure 9. Cytotoxicity of LLV. The cell viability was studied through MTT assay either for THP-1 or for J774 cells. The cells were exposed to the various particle systems (NPS, J774 LLV, THP-1 LLV) for 24 hours (cell/particle ratio = 1:20). The significance was calculated trough OneWay Anova analysis followed by Dunnet 's Test. All the standard deviations refer to three independent experiments with * = $p < 0.05$, ** = $p < 0.01$ ***= $p < 0.001$.

9. Assessment of untreated inflamed endothelial monolayer surface through SEM analysis
In order to investigate the superficial protuberances of the endothelial cells after treatment with NPS and LLV, we performed SEM analysis (**Figure 3A**). The internalization of LLV particles did not involve filopodia nor vesicle formation, leaving the cells at their initial unstimulated state (**Supplementary figure S10**)

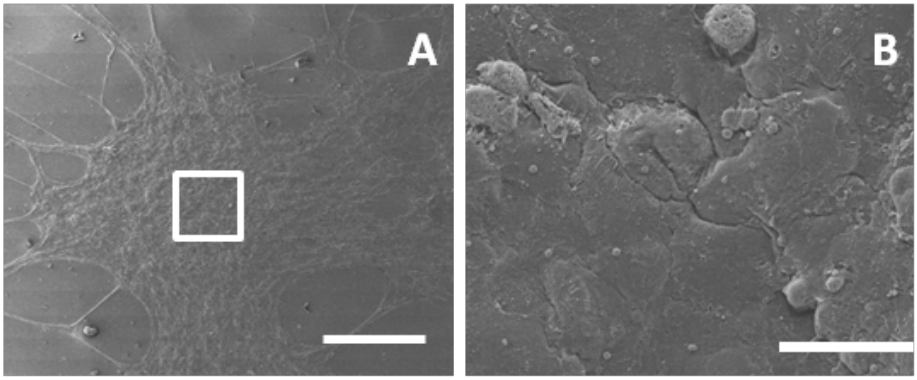

Supplementary figure 10. Evaluation untreated inflamed endothelial monolayer surface. A. Low magnification of untreated HUVECs seeded on matrigel and activated for 24 hours with TNF-α. The endothelial monolayer (white box) was also characterized by the formation of tube-like structures. **B.** High magnification of the endothelial monolayer showed in A. The surface of the endothelium appeared smooth and regular. No significant events of filopodia or vesicles were evident. Scale bar = 1 mm and 100 μm.

10. LFA-1 assessment on the LLV surface

The protocol used to assemble the system allowed the transfer of enriched cell membrane onto the surface of the NPS. LFA-1 is homogeneously distributed on the surface of the particles (**Supplementary figure S11**). The fluorometric analysis of this receptor displayed a slope of 15.48 for LLV against a slope of 3.192 for NPS (**Supplementary figure S11D)**.

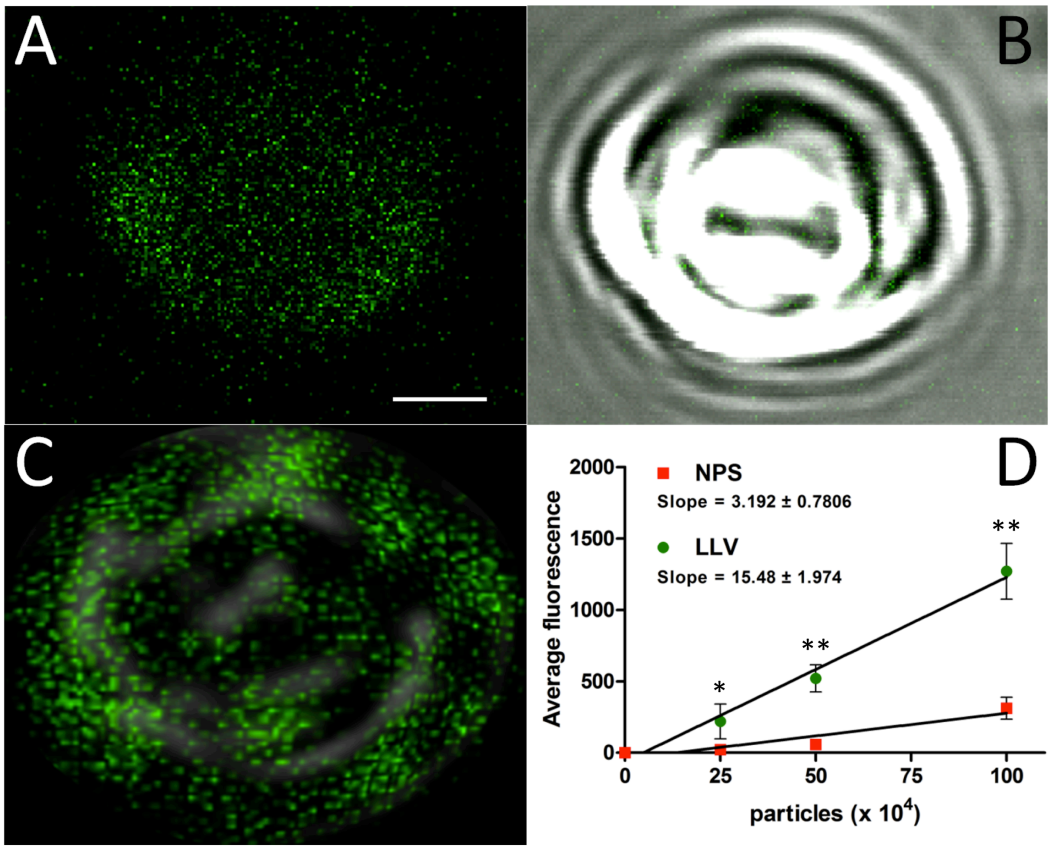

Supplementary figure S11. LFA-1 assessment and quantification on the surface of LLV. A. Confocal images of LLV particles immunostained for LFA-1 (green). Scale bar = 1 µm. **B.** Merged picture of the fluorescent and bright field. **C.** EDF reconstruction of the volume view. LFA-1 is evenly distributed onto the surface of LLV. **D.** Quantification of the staining through fluorimetric analysis expressed as slope of a standard curve reporting increasing concentration of NPS and LLV. * = $p < 0.05$, ** = $p < 0.01$.

11. Lysosomal Skipping and Intracellular Trafficking of NPS and LLV

In accordance with the data presented in **Figure 3F**, NPS were associated with lysosomes (stained with Lysotracker Red), while LLV were not found directly associated with these vesicles (**Figure 3F**). At early time points the quantification of the lysosomal activity indicated a significant increase (> 20 %) for cells treated with NPS versus untreated controls[69]. Upon LLV internalization, lysosomal activity was found unaltered, further confirming LLV endolysosomal avoidance during transport (**Supplementary figure S12A**) and thus supporting the potential use of LLV as carriers of bioactive payloads in the endothelial model. The lysosomal skipping performed by LLV was also confirmed assessing the lysosomal activity through intensity plots

(**Supplementary figure S12B**). NPS induced a significant increase in lysosomal activity compared to LLV that did not alter this parameter after 3 hours of treatment. After 24 hours, the lysosomal activity of cells treated with NPS and LLV were comparable to that of the untreated control (**Supplementary figure S12C-D**). These data showed that the activation of the lysosomal compartment due to NPS internalization is a reversible event, as previously shown for other types of particles[69] and confirmed the biocompatibility of this drug delivery tool[70]. The relative distribution of the particles inside and outside the endolysosomal vesicles confirmed the different compartmentalization of NPS and LLV after internalization. While the ~90% of NPS were founded inside cellular vesicle, only the ~25% of LLV were sequestered in the endolysosomal compartment (**Supplementary figure S13**).

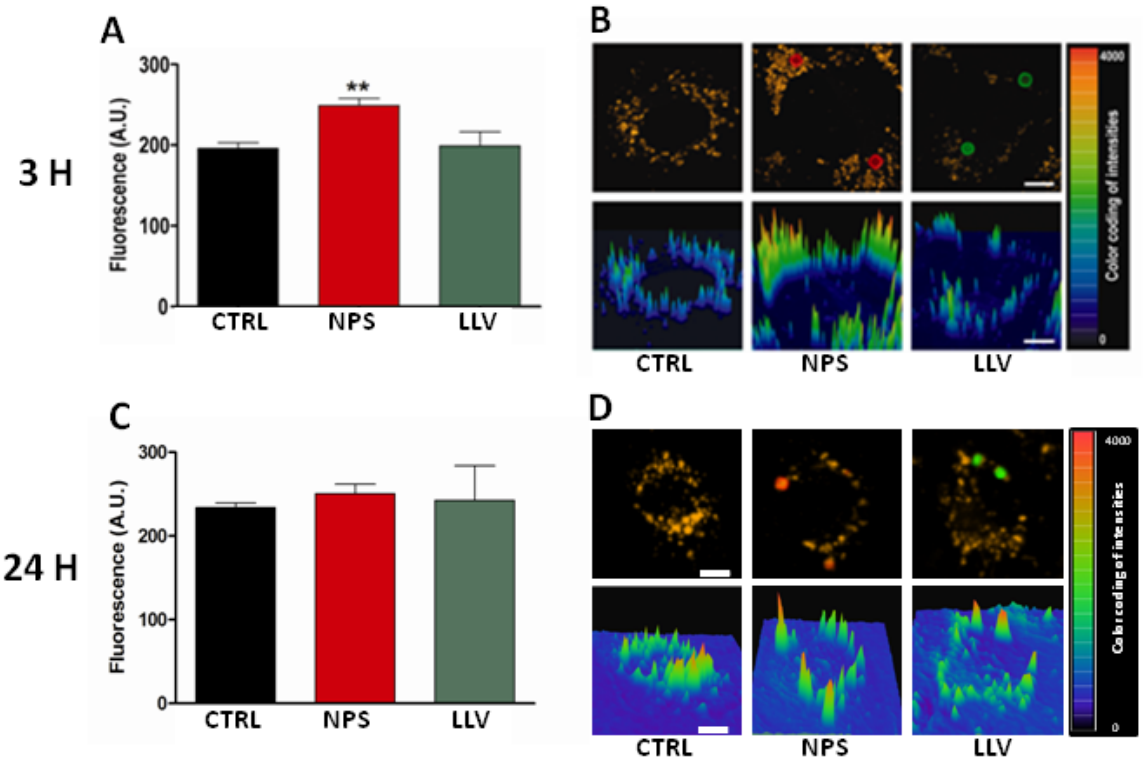

Supplementary figure S12. Lysosomal activity after incubation in an endothelial monolayer in inflammatory conditions. A. Quantification of the Lysotracker Red lysosomal staining detected in the confocal samples after 3 hour of incubation. Experiments were performed in triplicate and for each condition three fields were randomly chosen and analyzed. The significance was calculated through OneWay Anova analysis followed by Dunnett's Test. All the standard deviations refer to three independent experiments with ** = $p < 0.01$. **B.** Confocal images of inflamed endothelial cells seeded on fibronectin and incubated with NPS and LLV for 3 hours. The intensity plots showed the cellular lysosomal activity of untreated and NPS- and LLV-treated cells. Scale bar = 5 µm. **C.** Quantification of the Lysotracker Red lysosomal staining detected in the confocal samples after 24-hour incubation. Experiments were performed in triplicate and for each condition three fields were randomly chosen and analyzed. The significance was calculated through OneWay Anova analysis followed by Dunnett's Test. All the standard deviations refer to three independent experiments. **D.** Confocal images of inflamed endothelial cells seeded on fibronectin and incubated with NPS and LLV for 24 hours. The intensity plots showed the cellular lysosomal activity of untreated and NPS- and LLV-treated cells. Scale bar = 5 µm.

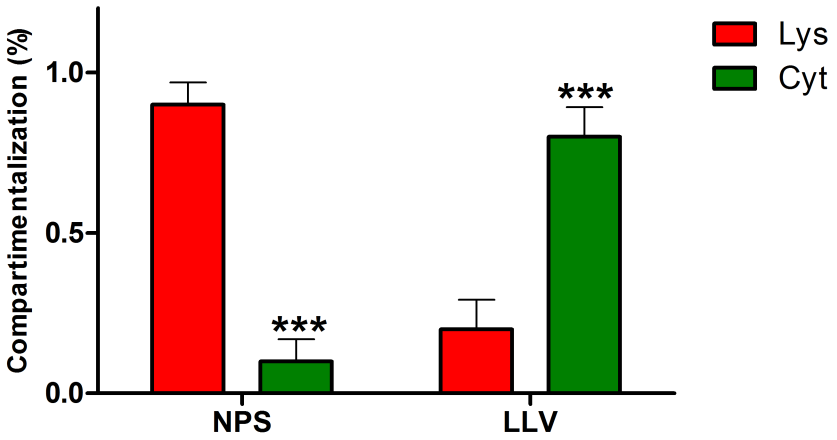

Supplementary figure S13. Relative distribution of NPS and LLV inside the endolysosomal compartment. TEM pictures were analyzed counting the particles inside and outside the endolysosomal compartment. The bars express the counted internalization events (n=20) and the relative distribution of the particles in cellular vesicles (red) and in the cytoplasm (green). ***= $p < 0.001$.

12. Transport quantification of NPS and LLV through a reconstructed endothelial monolayer

In order to quantify the ability of LLV to modulate vascular permeability of our *in vitro* system, we reconstructed an inflamed endothelium by seeding HUVEC on 8 µm porous transwell filters as previously described. After 3 hours of incubation the particles were counted in the supernatant, inside the cells, and at the bottom of the transwell system (**Supplementary figure S14A**). The data showed significant passive transport of the LLV on the other side of the transwell system (**Supplementary figure S14B**). However, we took into account that these devices were designed to establish surface interactions with leukocytes [71]. Therefore, we measured the differential retainment of the fibronectin coated filters treated with NPS and LLV and normalized the results (**Figure 4B**) accordingly. A standard curve related to the adhesion of the particles to the filter was built for NPS and LLV and the respective slopes were calculated (**Supplementary figure S14C**). The slopes were used to normalize the data obtained from the effective counts. This difference in filter affinity was significant.

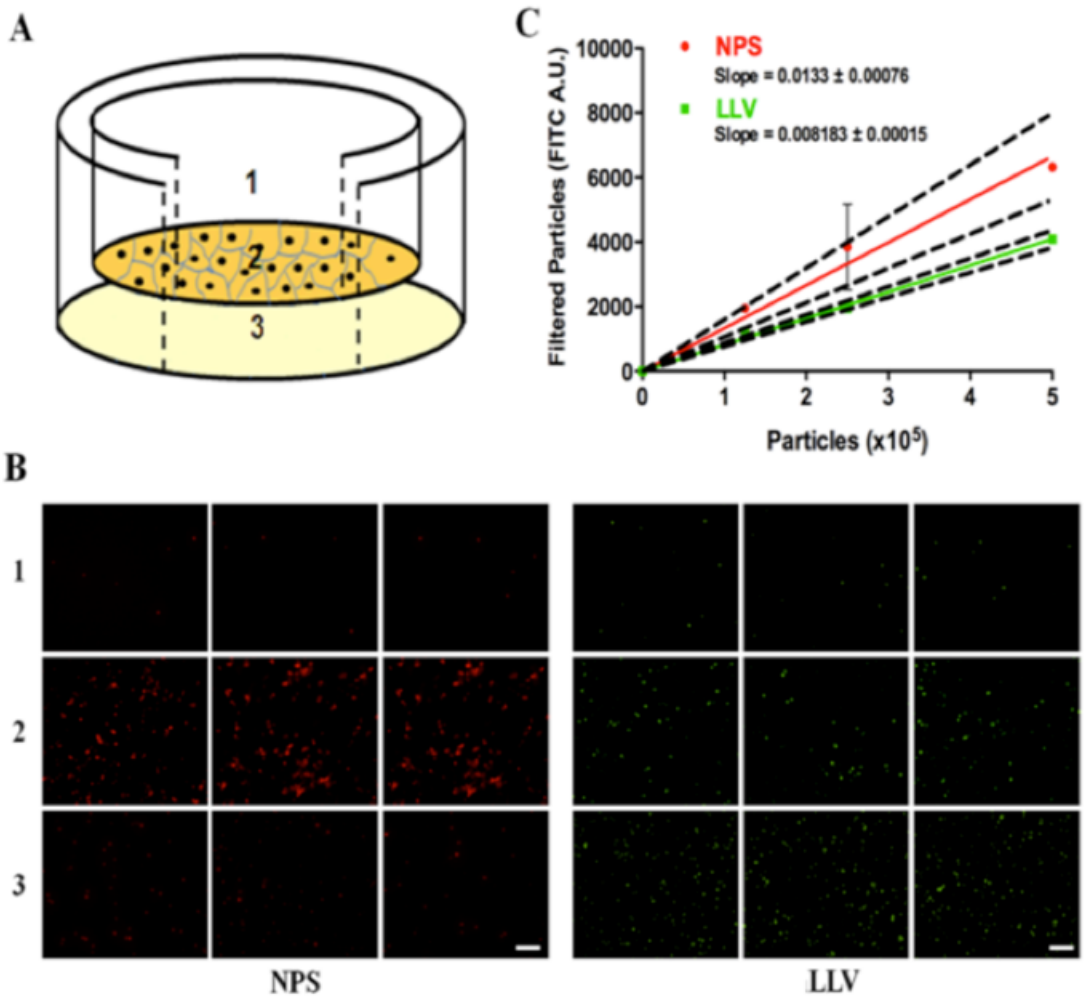

Supplementary figure S14. NPS and LLV transendothelial migration. A. Schematic of the experimental setup to quantify particle trasport: HUVEC were seeded over membrane insert filters with an 8 µm pore size coated with

fibronectin. The scheme represents the three compartments analyzed during the experiment: 1) supernatant, 2) filter, 3) bottom. **B.** Representative fluorescent microscope images of NPS and LLV found in the supernatant, in the HUVEC and at the bottom of the transwell after three hours of incubation. Scale bars = 50 μm. **C**. Standard curve of particle retention on the filter. Increasing concentrations of NPS and LLV were spotted on transwell filter coated with fibronectin. The filtered particles were counted and reported in the graph. For each sample, a trend line with the respective standard deviation was built.

Supplementary Material and Methods

Plasma Membrane Isolation

The source of the leukocyte membrane were J774, THP-1, and Jurkat cells that were continuously cultured and then cryopreserved. Preceding membrane isolation, preserved cells were thawed and then cultured for at least 24 hours. $2.8x10^8$ cells were centrifuged at 500 g for 10 min at 4 °C and the pellet resuspended in 2 mL of complete homogenization buffer (HB) (25mM sucrose, 10mM Tris/HCl, 1mM $MgCl_2$, 1mM KCl, 2mM phenylmethylsulfonyl fluoride (PMSF), trypsin-chymotrypsin inhibitor 200 μg/mL, DNase 10 μg/mL, RNase 10 ug/mL final concentration; Sigma-Aldrich) pH 7.3. Cells were enucleated in a hand-held Dounce homogenizer (20-30 passes while on ice) and centrifuged at 500 g for 10 min at 4 °C. The supernatant was collected and the pellet resuspended in HB. The homogenization and centrifugation steps were repeated until the pellet was free of intact cells, checked by light microscopy. The supernatants were pooled and laid on a discontinuous sucrose density gradient composed of 55 % (w/v), 40 % (w/v), 30 % (w/v) sucrose in a 0.9% normal saline solution (NSS). The discontinuous gradients were ultracentrifuged in a Beckman SW-28 rotor at 28,000 g for 30 min at 4 °C using polycarbonate tubes. The plasma membrane-rich region was collected at the 30/40% interface. Ten fractions were collected from the top to the bottom of the gradient for successive protein characterizations. The plasma membrane-rich region was diluted two-fold with NSS and ultracentrifuged in a Beckman SW-28 rotor at 28,000 g for 1 hour at 4 °C. The isolated membranes were lyophilized over night, weighed, rehydrated in NSS and stored at 4 °C.

Dot Blot Analysis

The distribution of proteins associated to nuclear, mitochondrial and plasma membranes along the gradient were analyzed by a dot-blot procedure. Briefly, 2.5 μL of each fraction were spotted on a polyvinylidene fluoride (PVDF) membrane. The membrane was blocked using a 5% milk and 0.1% Tween-20 TBS (tris-buffered saline) solution, followed by sequential incubation with primary antibodies (1:5000 dilution) against: anti nucleoporin p62 (Np62), cytochrome c oxidase subunit IV (COX IV), lymphocyte-specific protein tyrosine kinase (Lck), CD45, CD3z (SantaCruz Biotecnology) and lymphocyte function-associated antigen 1 (LFA-1 or CD11a) (Biolegend), and HRP (Horseradish Peroxidase) conjugated mouse anti-human IgG secondary antibody (1:10000 dilution) (Santa Cruz Biotechnology). The blots were developed using SuperSignal West Dura chemiluminescent substrate (Pierce) and the luminescent signals recorded on X-ray film using a Konica SRX-101A X-ray processor.

Analysis of NPS Size Distribution and Particle Counts

The size distribution and particle count were determined using a Multisizer 4 Coulter Counter Analyzer (Beckman Coulter, Fullerton, CA). The samples were diluted in the balanced electrolyte solution (ISOTON II Diluent, Beckman Coulter, CA) and dispersed by sonication for 4 seconds before analysis, as reported in Tasciotti et al.[72].

Zeta Potential Analysis

The zeta potential values of all the samples were analyzed using a Zetasizer nano ZS (Malvern Instruments Ltd., Southborough, MA). The zeta potential values of NPS, LLV, lipid membrane solutions and cells were evaluated by diluting a suspension of 2×10^5 particles or cells into 1.4

mL of phosphate buffer pH 7.3 contained in a sample cell countering according to Tasciotti et al.[72]. For each sample, the analysis was performed in triplicate at room temperature.

Leukolike Vector Assembly

The protein concentration of the isolated plasma membranes was quantified using a Bradford assay (BioRad) (data not shown). The lipid concentration was estimated considering the protein to lipid ratio 1:1 by weight. The membrane solutions were diluted to have a final lipid concentration of 1 mg/mL. Lipid membrane solutions with a dilution factor of 1:2 and 1:5 were also prepared. NPS ($1.5x10^6$) with a diameter of 2.8 μm, oxidized or APTES modified, were incubated with the lipid membrane solution over night at 4°C, under continuous rotation. After incubation, the unbound membranes were washed away from the membrane-cloaked-NPS (LLV) by centrifugation at 1000 rpm for 10 min. The same conditions were applied for all the LLV types.

Fourier Transform Infrared (FT-IR)

FT-IR spectra were obtained on a Nicolet 6700 spectrometer (Thermo Scientific,Waltham, MA) with a deuterated triglycine sulfate (DTGS) detector and potassium bromide (KBr) beam splitter. Typically, 64 scans were performed in the wavenumber range of 4000–600/cm, both forward and backward at 4 kHz, with a manual gain of one. Pellets of 5×10^6 particles of each sample (NPS and LLV) and about 100mg KBr (spectroscopy grade, Acros Organics) were pressed using a Carver laboratory press. Spectra were collected by transmitting IR light through the pellets.

Thermogravimetric analysis (TGA)

TGA of NPS and LLV was performed using a Q600 SDT (TA Instruments Inc., New Castle, DE) by heating the samples dispersed in water from 30 ºC to 150 ºC in a nitrogen atmosphere at a rate of 10 ºC. $5x10^6$ particles of each sample (NPS and LLV) were submerged into PBS at 37 ºC for 1 hour and 24 hours before the analysis. The particles were separated from PBS by centrifugation and were re-dispersed in 50 μL of water during the TGA study.

Flow Cytometry Analysis of LLV Protein Profile

A surface staining of Jurkat cells (1x10^6), NPS (2x10^6) and LLV (2x10^6) was performed to determine the presence of specific proteins. The samples were incubated with primary labeled monoclonal antibodies, FITC-conjugated anti-CD3z mAb (Santa Cruz Biotechnology; CA) or APC-conjugated anti-CD11a mAb (Biolegend; US), in ice-cold PBS, 10% FBS, 1% sodium azide pH 7.2, for 1 hour, in the dark, under continuous rotation. For the intracellular staining of the CD3z domain, Jurkat cells were previously permeabilized with 0.01% Tween-20 (Sigma; US) in PBS for 4 min. IgG FITC- and APC-conjugated mAb isotypes were used as controls at the same experimental conditions. After incubation, the unreacted mAb were removed by centrifugation and the samples were analyzed with a Becton Dickinson LSR Fortessa equipped with Diva software. Five thousand events were evaluated for each experiment. The results were the average of three independent experiments.

Time Lapse Imaging (TLM) of LLV Interactions with Macrophages

TLM was performed at TMHRI Advanced Cellular and Tissue Microscope Core Facility using a Spinning Disk Confocal microscope (Olympus) equipped with an incubation chamber that maintained imaging conditions at 37 °C and 5% CO_2. J774 and THP-1 phagocytic cells were

seeded in chamber slides and treated with 5 and 10 particles/cell (labeled with Alexafluor 555), respectively. The THP-1 cell line was previously activated with 100ng/mL of phorbol myristate acetate for 24 hours prior to TLM. Images were acquired every 6 minutes using a 40x objective for 4 hours. At each imaging point the DIC and TRITC channels were collected and analyzed with Slidebook software to generate movies.

LLV Loading and Release Profile of a Payload

APTES-NPS (1×10^8, 2.8 μm) were resuspended into 200 μL of a FITC-conjugated bovine serum albumin (FITC-BSA) solution (5mg/mL) for 2 hours at 4 °C in the dark, under continuous rotation. Samples were then centrifuged at 2000 rpm (Beckman Coulter Allegra X-22 Centrifuge equipped with a 296/06 rotor) for 5 minutes to remove the free unloaded FITC-BSA. The amount of FITC-BSA in the supernatant was quantified by evaluating its emission peak at 488 nm using a UV-vis spectrophotometer. The fluorescence was converted into a concentration (μg/mL) of BSA using standard curves obtained at known FITC-BSA concentrations. The FITC-BSA loaded NPS were mixed with 200 μL of 1 mg/mL coating membrane solution and incubated at 4 °C for 2 hours under continuous rotation. FITC-BSA loaded NPS used as controls were subjected to the same procedure. Samples were then centrifuged at 1000 rpm for 5 minutes to remove the unbounded membranes and the amount of FITC released during the coating step. The amount of loaded FITC-BSA left in NPS and LLV was then estimated by spectrophotometry.

The release profile of FITC-BSA from NPS and LLV was evaluated maintaining the systems in a moving condition. The supernatants were taken out at an established time (30 min, 1, 3, 24, & 48 hours) and replaced with 200 μL fresh PBS. The fluorescence of FITC-BSA at 488 nm was reported and the cumulative release of FITC-BSA was calculated. Statistical analysis of the release from the two different systems (NPS/LLV) was then conducted. T-Test analysis were carried out and $p < 0.5$ was used as a significant level. The same procedures were applied to determine the loading and release profile of Doxorubicin (DOX). The DOX loading solution had a concentration of 2 μg/mL with an absorbance peak at 490 nm.

Scanning and Transmission Electron Microscopy.

HUVEC were seeded at 80,000 cells/filter on ThinCerts™ inserts coated with matrigel or fibronectin and co-incubated with NPS or Jurkat LLV for 15, 60 minutes (SEM) and 6 hours (TEM). After treatment, the samples were fixed and prepared for SEM and TEM as described in the published study.[70] Samples were sputter-coated with a 5 nm layer of gold and imaged using an FEI quanta 400 ESEM FEG instrument equipped with an ETD (SE) detector or a Hitachi S-5500 SEM apparatus.

Flow Chamber Experiments.

HUVEC cells were seeded onto fibronectin-coated flow cells (Ibidi μ-slide) at a density of 1.25×10^6 cells/ml with or without media containing TNF-α (0.1μg/mL). 24 hours later, 3×10^7 NPS or Jurkat-LLV, were introduced into the flow cell at a rate of 0.5 dyn/cm^2 for 1 hour. Cells were subsequently fixed and prepared for microscopy as described above.

Flow Cytometry.

J774 cells were seeded at 30 % confluence in 25cm^2 flasks and co-incubated with NPS, THP-1 LLV, or J774 LLV (tagged with DyLight 549 or PE-Rhod respectively) at cell: particle ratios of

1:5. After 3 hours, samples were washed twice in PBS to remove non-adherent particles. Cells were harvested by scraping and treated with Trypan Blue (0.04 % v/v) to quench their surface fluorescence. The same experiment conditions were applied to study the internalization of Human THP-1 cells. In this experiment, the cells were activated with 100ng/mL phorbol myristate acetate (Sigma Aldrich) and the cells were treated at a cell: particle ratio of 1:20. Flow cytometry was performed using a BD LSR Fortessa equipped with Diva software and quantified using FlowJo.

Supplementary table 1

	Zeta Potential (mV)	Mobility (µmcm/Vs)
Leukocyte membranes	-26.44 ± 1.40	-1.97 ± 0.10
NPS	-28.84 ± 2.49	-2.17 ± 0.19
APTES-NPS	7.41 ± 1.16	0.56 ± 0.09
LLV	-26.00 ± 1.50	-1.70 ± 0.45
Jurkat cells	-31.16 ± 0.68	-2.34 ± 0.05
J774 cells	-35.5 ± 1.71	-2.125 ± 0.13

Supplementary Table 1. Zeta Potential analysis. Zeta potential values of leukocyte membranes, oxidized NPS, APTES-NPS, LLV, Jurkat and macrophage cells. The zeta potential values were measured as a function of the electrophoretic mobility (µmcm/Vs). Data are the average of three different experiments ± standard deviation.

Supplementary equations S1-2, based on NPS transport rate were used to calculate the data shown in **Figure 4B** relative to LLV transport in inflammatory conditions. The same analysis was performed in the experiments run without TNF-α.

Supplementary equation S1

$$I_{LLV} = \frac{N_{LLV}^{i} \cdot m_{LLV}}{m_{NPS}}$$

where I_{LLV} is the correct number of intracellular LLV, $N_{LLV}^{i}$is the number of intracellular LLV counted, m_{LLV} is the slope of the LLV regression, and m_{NPS} is the slope of the NPS regression.

Supplementary equation S2

$$F_{LLV} = \frac{N_{LLV}^{f} \cdot m_{LLV}}{m_{NPS}}$$

where F_{LLV} is the correct number of filtered LLV, N_{LLV}^{f} is the number of filtered LLV counted, m_{LLV} is the slope of the LLV regression, and m_{NPS} is the slope of the NPS regression.

Supplementary Movie Legends

Supplementary movie S1-6. Interaction of Phagocytic cells with NPS, J774 LLV and THP-1 LLV. The movies were produced using Slidebook after acquisition on an inverted Olympus for more than 240 min of continuous imaging every six minutes. The movies depict the interactions between human THP-1 monocytic cells (Supplementary movie S1-3) and murine J774 macrophages (Supplementary movie S4-6) upon exposure with NPS (red), J774 LLV (orange) and THP-1 LLV (green). In particular, THP-1 LLV particles displayed significantly less ameboid movements and internalization compared to NPS particles upon interacting with THP-1. On the other hand, J774 LLV demonstrated similar interactions as above with minimal internalization compared to NPS particles. (.mov; 6.7, 5.1, 3.8, 4.3, 4.9, 5.2 MB).

Supplementary movies S7-8. Cytoskeleton Reorganization of In Vitro Reconstructed Endothelium after Treatment with NPS and LLV. HUVECs were seeded at 50-75x10^4 cells per filter (porosity 8 μm) on fibronectin and pretreated wit TNF-α. The movies represent cells positive for actin staining (red) and nuclear staining (blue). The cells were treated with NPS (red) and LLV (green). Details of the actin-organization during particle internalization and TM are displayed via stacks of 58 images. The movies show 3D reconstructed volume-views of the zeta-stack images taken on the Nikon A1 system following AutoQuant Deconvolution (.mpg, 15.2 MB and 15.8 MB respectively).

References.

51 Tadevosyan, A. *et al.* Nuclear-delimited angiotensin receptor-mediated signaling regulates cardiomyocyte gene expression. *J. Biol. Chem.* **285**, 22338-22349 (2010).

52 Shen, Y. *et al.* Mitochondria-dependent apoptosis of activated t lymphocytes induced by astin c, a plant cyclopeptide, for preventing murine experimental colitis. *Biochem. Pharmacol.* **82**, 260-268 (2011).

53 Donovan, J. A. & Koretzky, G. A. Cd45 and the immune response. *J. Am. Soc. Nephrol.* **4**, 976-985 (1993).

54 van Vliet, S. J., Gringhuis, S. I., Geijtenbeek, T. B. & van Kooyk, Y. Regulation of effector t cells by antigen-presenting cells via interaction of the c-type lectin mgl with cd45. *Nat. Immunol.* **7**, 1200-1208 (2006).

55 Huang, S. C., Tsai, H. F., Tzeng, H. T., Liao, H. J. & Hsu, P. N. Lipid raft assembly and lck recruitment in trail costimulation mediates nf-kappab activation and t cell proliferation. *J. Immunol.* **186**, 931-939 (2011).

56 Berg, L., Ronnelid, J., Klareskog, L. & Bucht, A. Down-regulation of the t cell receptor cd3 ζ chain in rheumatoid arthritis (RA) and its influence on t cell responsiveness. *Clin. Exp. Immunol.* **120**, 174-182 (2000).

57 Roy, S. *et al.* Novel multiparametric approach to elucidate the surface amine-silanization reaction profile on fluorescent silica nanoparticles. *Langmuir.* **26**, 18125-18134 (2010).

58 Maria Chong, A. S. & Zhao, X. S. Functionalization of sba-15 with APTES and characterization of functionalized materials. *J. Phys. Chem. B.* **107**, 12650-12657 (2003).

59 Kulikova, G. A. *et al.* In vitro studies of interaction of modified silica nanoparticles with different types of immunocompetent cells. *J. Biomed. Mater. Res. A.* **95A**, 434-439 (2010).

60 Kim, J., Cho, J., Seidler, P. M., Kurland, N. E. & Yadavalli, V. K. Investigations of chemical modifications of amino-terminated organic films on silicon substrates and controlled protein immobilization. *Langmuir.* **26**, 2599-2608 (2010).

61 Bonasio, R. *et al.* Specific and covalent labeling of a membrane protein with organic fluorochromes and quantum dots. *Proc. Natl. Acad. Sci.* **104**, 14753-14758 (2007).

62 Levin, S. E. & Weiss, A. Twisting tails exposed: The evidence for tcr conformational change. *J. Exp. Med.* **201**, 489-492 (2005).

63 Tanaka, T. *et al.* Sustained small interfering RNA delivery by mesoporous silicon particles for cancer treatment. *Cancer Res.* **70,** 3687-3696 (2010).

64 Ferrari, M. Cancer nanotechnology: Opportunities and challenges. *Nat. Rev. Cancer.* **5**, 161-171 (2005).

65 Ferrari, M. Frontiers in cancer nanomedicine: Directing mass transport through biological barriers. *Trends Biotechnol.* **28**, 181-188 (2010).

66 Fan, D. *et al.* Mesoporous silicon-plga composite microspheres for the double controlled release of biomolecules for orthopedic tissue engineering. *Adv. Func. Mater.* **22**, 229-229 (2012).

67 De Rosa, E. *et al.* Agarose surface coating influences intracellular accumulation and enhances payload stability of a nano-delivery system. *Pharm. Res.* **28**, 1520-1530 (2011).

68 Osterloh, K., Ewert, U. & Pries, A. R. Interaction of albumin with the endothelial cell surface. *Am. J. Physiol. Heart Circ. Physiol.* **283**, 398-405 (2002).

69 Albini, A. *et al.* Interactions of single-wall carbon nanotubes with endothelial cells. *Nanomedicine.* **6**, 277-288 (2010).

70 Serda, R. E. *et al.* Mitotic trafficking of silicon microparticles. *Nanoscale.* **1**, 250-259 (2009).

71 Forde, S. *et al.* Endolyn (cd164) modulates the cxcl12-mediated migration of umbilical cord blood cd133+ cells. *Blood.* **109**, 1825-1833 (2007).

72 Tasciotti, E. *et al.* Near-infrared imaging method for the in vivo assessment of the biodistribution of nanoporous silicon particles. *Mol. Imaging.* **10**, 56-68 (2011).